

Low temperature studies of the removal reactions of $^1\text{CH}_2$ with particular relevance to the atmosphere of Titan



Kevin Douglas^a, Mark A. Blitz^{a,b}, Wuhu Feng^{a,b}, Dwayne E. Heard^{a,b}, John M.C. Plane^{a,b}, Eloise Slater^a, Karen Willacy^c, Paul W. Seakins^{a,b,*}

^a School of Chemistry, University of Leeds, Leeds, LS2 9JT, UK

^b National Centre for Atmospheric Science (NCAS), University of Leeds, Leeds, LS2 9JT, UK

^c CALTECH, Jet Prop Lab, 4800 Oak Grove Dr, Pasadena, CA 91109 USA

ARTICLE INFO

Article history:

Received 6 April 2017

Revised 27 October 2017

Accepted 13 December 2017

Available online 14 December 2017

ABSTRACT

Methylene, CH_2 , is one of the major photolysis products of methane by Lyman- α radiation and is involved in the photochemistry of the atmospheres of Titan and the giant planets. The kinetics of the reactions of the first excited state of methylene, $^1\text{CH}_2$, with He, N_2 , O_2 , H_2 and CH_4 have been measured over the temperature range 43–160 K by pulsed laser photolysis, monitoring $^1\text{CH}_2$ removal by laser induced fluorescence. Low temperatures were obtained with either a pulsed Laval expansion (43–134 K) or a, slow flow reaction cell (160 K). The rate coefficients for the reactions with N_2 , O_2 , H_2 and CH_4 all showed a strong negative temperature dependence. In combination with other literature data, the rate coefficients can be parameterised as:

$$k_{\text{He}}(43 < T/\text{K} < 800) = (1.90 \pm 0.23) \times 10^{-12} \times (T/298)^{1.74 \pm 0.16} \times \exp^{(88 \pm 23)/T}$$

$$k_{\text{N}_2}(43 < T/\text{K} < 800) = (2.29 \pm 1.12) \times 10^{-12} \times (T/298)^{-2.15 \pm 1.38} \times \exp^{(-74 \pm 96)/T} \\ + (3.91 \pm 0.78) \times 10^{-11} \times \exp^{(-469 \pm 114)/T}$$

$$k_{\text{O}_2}(43 < T/\text{K} < 300) = (6.16 \pm 1.09) \times 10^{-11} \times (T/298)^{-0.65 \pm 0.14}$$

$$k_{\text{H}_2}(43 < T/\text{K} < 800) = (1.10 \pm 0.04) \times 10^{-10} \times (T/298)^{-0.40 \pm 0.06} \times \exp^{(11.1 \pm 6.9)/T}$$

$$k_{\text{CH}_4}(43 < T/\text{K} < 475) = (8.20 \pm 0.46) \times 10^{-11} \times (T/298)^{-0.93 \pm 0.10} \times \exp^{(-20.5 \pm 12.8)/T}$$

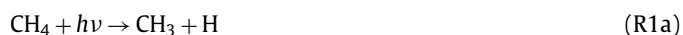
For the reactions of $^1\text{CH}_2$ with H_2 and CH_4 , the branching ratio for quenching to ground state, $^3\text{CH}_2$, vs chemical reaction was also determined at 160 and 73 K. The values measured (H_2 : 0.39 ± 0.10 at 160 K, 0.78 ± 0.15 at 73 K; CH_4 : 0.49 ± 0.09 at 160 K, 0.64 ± 0.19 at 73 K) confirm trends of an increased proportion of reactive loss with increasing temperature determined at higher temperatures. The impacts of the new measurements for Titan's atmosphere have been ascertained using a 1D chemistry and transport model. A significant decrease ($\sim 40\%$) in the mixing ratio of ethane between 800 and 1550 km is calculated due to the decrease contribution of methyl production from the reaction of $^1\text{CH}_2$ with CH_4 , with smaller increases in the concentrations of ethene and acetylene. Ethene production is enhanced by more methylene being converted to methylidene, CH, and the subsequent reaction of CH with CH_4 to generate ethene. Photolysis of ethene is the major route to acetylene formation.

© 2018 The Authors. Published by Elsevier Inc.

This is an open access article under the CC BY license. (<http://creativecommons.org/licenses/by/4.0/>)

1. Introduction

The photolysis of methane by UV photons is the primary source of hydrocarbon radicals in the atmospheres of Titan and the giant planets. The photolysis channels are thought to be (Blitz and Seakins, 2012):



However, there is still significant uncertainty in the branching ratios as a function of wavelength e.g. (Gans et al., 2011) and implications of methane photolysis pathways on subsequent chemistry (Blitz and Seakins, 2012; Wilson and Atreya, 2000). Methylene, CH_2 , is an important product and can be produced in either the triplet groundstate ($^3\text{CH}_2$, X^3B_1) or the first excited singlet

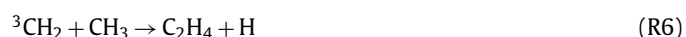
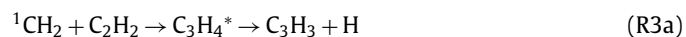
* Corresponding author.

E-mail address: p.w.seakins@leeds.ac.uk (P.W. Seakins).

state ($^1\text{CH}_2$ a $^1\text{A}_1$). Estimates of the yields of $^1\text{CH}_2$ at the dominant Lyman- α (121.6 nm) wavelength range from 0 to 0.53 (Mordaunt et al., 1993; Smith and Aaulin, 1999). Photolysis of CH_3 (R2) is a further source of $^1\text{CH}_2$.



Although the energy gap between the ground and first excited states of methylene is small (37.7 kJ mol $^{-1}$ (Jensen and Bunker, 1988)) compared to the high heats of formation, the chemistries of the two species are quite different. $^1\text{CH}_2$ rapidly inserts into bonds followed by dissociation of the chemically activated intermediate (e.g. R3a, R4a), whereas $^3\text{CH}_2$ is relatively unreactive with closed shell molecules and the major loss processes are reactions with radical species such as H (R5) and CH_3 (R6):



The reaction of $^1\text{CH}_2$ with acetylene (R3) leads to the formation of the propargyl radical, C_3H_3 , and has been proposed as an important radical route to benzene, C_6H_6 , formation on Titan (Wilson and Atreya, 2003), with benzene being the first step in the formation of the layer of tholin aerosols at 300–400 km above the surface of Titan (Lorenz, 2014). Reaction R5 is an important source of CH, methylidene, radicals; on Titan the primary loss of CH is via reaction with methane (R7) leading to the formation of unsaturated species such as ethylene and acetylene (R8) (Blitz et al., 1997; Canosa et al., 1997; Thiesemann et al., 1997):



Both methylene species are therefore important in different aspects of Titan's complex photochemistry.

In the atmospheres of the giant planets, methane photolysis is still the main source of hydrocarbon radicals, but $^1\text{CH}_2$ chemistry is dominated by reaction with molecular hydrogen (R9) (Gannon et al., 2008; Hancock and Heal, 1992; Wagener, 1990):



For the reactions of $^1\text{CH}_2$ there is a parallel relaxation process in which collisions with C_2H_2 , CH_4 , H_2 , and other molecular species lead to ground state $^3\text{CH}_2$:



Measurements around 300 K suggest that relaxation is $\sim 20\%$ of the overall loss process for $^1\text{CH}_2$ reactions with C_2H_2 , CH_4 and H_2 (Böhland et al., 1985; Gannon et al., 2010b,c, 2008). The competition between reaction and relaxation has been studied in this laboratory as a function of temperature between 195 and ~ 500 K monitoring the H atom yield from reactions (3) and (9) (Gannon et al., 2010b,c, 2008). Gannon et al. (2010c) showed that the fraction of reactive loss decreased from $\sim 100\%$ at 500 K to $\sim 30\%$ by 195 K

for the reactions of $^1\text{CH}_2$ with acetylene and ethylene, suggesting that at the temperatures of Titan's photochemically active stratosphere (70–170 K), relaxation to $^3\text{CH}_2$ should be the dominant process. However, no direct measurements have been made at these temperatures.

Cui et al. (2009) reported that $\sim 96.6\%$ of Titan's atmosphere is nitrogen at 1150 km, with CH_4 and H_2 accounting for ~ 3.0 and $\sim 0.4\%$ of the composition, respectively. For the reactions of $^1\text{CH}_2$ with nitrogen (R10) and the monotonic rare gases, relaxation is the only possible loss process. The temperature dependence and mechanism of the reaction of $^1\text{CH}_2$ with the rare gases and N_2 has also been studied by Gannon et al. (2010a). A positive temperature dependence was observed in the rate coefficient for collisional deactivation between 195 and 700 K consistent with earlier work (Hayes et al., 1996; Wagener, 1990) and selective monitoring of the ortho- and para-states in $^1\text{CH}_2$ provided the first direct confirmation that such processes occur via a gateway mechanism between near co-incident states in the singlet and triplet manifolds of methylene (Bley and Temps, 1993). Extrapolation of the rate coefficients from Gannon et al. (2010a) to the 70–170 K range relevant to Titan and the upper atmospheres of the giant planets would suggest a decreased contribution of the role of N_2 (R10) or He (R11) in removing $^1\text{CH}_2$.



Chemical models of Titan's atmosphere deal with methylene chemistry in varying levels of detail. In some models only the reactions of $^1\text{CH}_2$ with N_2 , CH_4 and H_2 are considered and, as many models were constructed before the measurements of Gannon et al., they do not all include the temperature dependence of $^1\text{CH}_2$ reactions and some ignore the role of relaxation, a minor contribution at room temperature. The way in which various models consider reactions R4, R9 and R10 is discussed later.

In the present paper we report a study of several of the relevant reactions under pertinent conditions for modelling Titan's stratospheric chemistry. The rate coefficients for the reactions of $^1\text{CH}_2$ with He, N_2 , O_2 , H_2 , and CH_4 have been measured between 40 and 160 K by pulsed laser photolysis (PLP) to generate $^1\text{CH}_2$ with the removal of $^1\text{CH}_2$ being monitored by laser induced fluorescence (LIF) in two separate experiments, using either a pulsed Laval nozzle apparatus (40–134 K), or a low temperature reaction cell (160 K). In addition, for the reactions of $^1\text{CH}_2$ with CH_4 and H_2 , the branching ratio between reaction and relaxation has been determined at 80 and 160 K. A separate paper will report results on the reactions of $^1\text{CH}_2$ with C_2H_2 , C_2H_4 , and C_2H_6 .

2. Experimental methods

All studies were carried out by PLP LIF detection, of either the $^1\text{CH}_2$ reagent or OH product. Measurements of rate coefficients and branching ratios between 40 and 125 K were carried out using a pulsed Laval nozzle apparatus. The use of a Laval nozzle expansion to study low temperature reactions was first demonstrated by Rowe and co-workers, who used the technique to study ion-molecule reactions (Rowe and Marquette, 1987). The technique was later adopted for the study of neutral-neutral reactions by the use of PLP-LIF (Brownsword et al., 1997; Canosa et al., 1997), and has since enjoyed considerable success, and has been extensively reviewed (Sims and Smith, 1995; Smith, 2006; Smith et al., 2006). The pulsed Laval nozzle apparatus employed in this study has been discussed in detail in recent publications (Caravan et al., 2015; Gomez Martin et al., 2014; Shannon et al., 2013, 2010; Taylor et al., 2008), so only a brief description is given

Table 1
Characteristics of Laval nozzle gas expansions used in this study.

T (K)	Bath gas M	[M] (10^{16} molecule cm^{-3})
43 ± 7	He	5.5 ± 1.4
		6.9 ± 2.1
		8.1 ± 2.4
		10.0 ± 2.0
73 ± 10	He	12.7 ± 2.2
		17.8 ± 3.5
		22.4 ± 5.0
		13.2 ± 3.2
84 ± 15	He	18.4 ± 5.2
		24.1 ± 7.0
		2.0 ± 0.5
		3.2 ± 0.7
124 ± 11	N ₂	5.5 ± 1.4
		3.2 ± 1.1
		5.3 ± 2.0
		10.0 ± 4.6
134 ± 21	N ₂	2.0–10.0 (± 5%)

^a Range of conditions used in reaction cell experiments.

here. The reaction mixture consisting of radical precursor, reagent, and bath gas, was introduced to a 1 cm³ stainless steel reservoir via two pulsed solenoid valves (Parker 9 Series), fired at a 5 Hz repetition frequency with a pulse duration of between 10 and 20 ms, depending on the Laval nozzle employed. The gas mixture was then expanded through the convergent-divergent shaped Laval nozzle into a low pressure stainless steel cylindrical chamber (774 mm length × 240 mm diameter), producing a thermally equilibrated, low temperature jet. The temperature and density profile of the jet were characterized by impact pressure measurements, and the temperature also by rotationally resolved laser-induced fluorescence spectroscopy. The properties of the characterized expansions used in this study are given in Table 1.

Ketene, the ¹CH₂ precursor, was generated by pyrolysis of acetic anhydride (> 99%, Alfa Aesar) (Fisher et al., 1953), purified by trap-to-trap distillation and diluted in a cylinder with the bath gas (He or N₂), and the purity checked by IR spectroscopy (Arendale and Fletcher, 1957). Reagent and bath gases used were all of analytical quality (He 99.995%, N₂ 99.9992%, O₂ 99.5%, H₂ 99.99%, CH₄ > 99.9%, all BOC gases). Reaction gas mixtures were obtained by flowing the relevant gases through calibrated mass flow controllers (MFCs) (MKS Instruments) and allowing mixing in a 1 L ballast tank prior to the pulsed solenoid valves. The photolysis laser was introduced collinearly with the axis of the expanded gas flow, to produce a uniform radical density. The probe laser was introduced perpendicularly to photolysis laser beam, and the fluorescence collected via a series of lenses and observed with a photomultiplier tube (Thorn EMI) mounted at 90° to both laser beams.

Measurements of rate coefficients and branching ratios at 160 K were carried out in a low temperature slow-flow reaction cell apparatus. The reaction cell is a six-way stainless steel cross that was cooled by immersion into a bath of dry ice/ethanol. Temperatures around the observation region were monitored using a thermocouple. Preparation of the ¹CH₂ precursor, ketene, and the reagent and bath gases used, was as detailed above. Reaction gas mixtures were obtained by flowing the relevant gases through calibrated MFCs (MKS Instruments) and combining in a stainless steel transfer line before introduction into the cell. The total flow rate was sufficient to ensure a fresh flow of gas into the cell for each photolysis laser pulse. The total pressure, as measured by two gauges (0–10 Torr and 0–100 Torr baratron), was controlled by a valve on the exit line to the pump. The photolysis and probe laser beams were introduced collinearly on opposite sides of the cell, so as to obtain maximum overlap in the observation region. Fluorescence was observed with a photomultiplier tube (Thorn EMI) mounted at 90° to the laser beams.

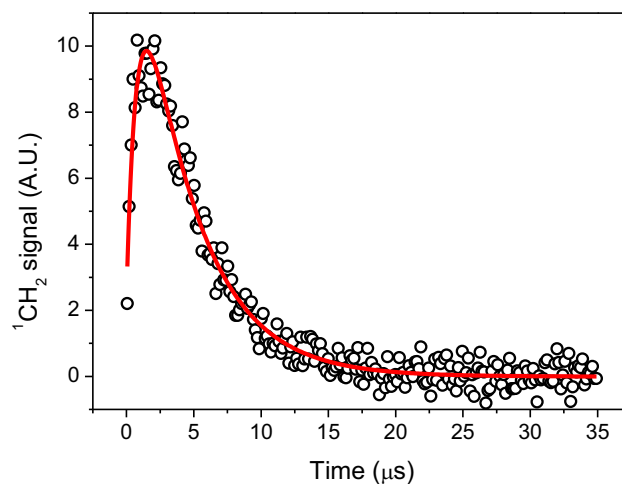
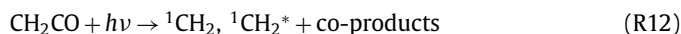


Fig. 1. Temporal evolution of the ¹CH₂ LIF signal (black open circles) together with the nonlinear least-squares fit of Eq. E1 to the data (red line) following 308 nm photolysis of ketene in the presence of [H₂] = 6.0 × 10¹⁴ molecule cm⁻³ [total density (1.0 ± 0.2) × 10¹⁷ molecule cm⁻³ in He, T = (43 ± 7) K, fit gives $k_{\text{obs}} = (243.2 \pm 9.1) \times 10^3 \text{ s}^{-1}$]. (For interpretation of the references to colour in this figure legend, the reader is referred to the web version of this article.)

2.1. Rate coefficient measurements

For both experiments, the rate coefficients for the reaction of ¹CH₂ with co-reactants He (R11), N₂ (R10), O₂ (R15), H₂ (R9), and CH₄ (R4) were measured by monitoring the temporal decay of the ¹CH₂ radical via PLP-LIF. The experiments were performed under pseudo-first-order conditions so that the concentration of the co-reagent was in great excess of the ¹CH₂ concentration. ¹CH₂ was produced by the pulsed photolysis of ketene at 308 nm (Lambda Physik LPX100). The photolysis mechanism is well established at this wavelength, with > 95% of the methylene produced being in the required singlet state (Morgan et al., 1996; Wade et al., 1997). The subsequent decay of ¹CH₂ due to reaction and other loss processes was measured by probing the b¹B₁ ← a¹A₁ transition at either ~590.7 nm or ~653.3 nm using light from an excimer pumped dye laser (Lambda Physik LPX100 pumping a Lambda Physik FL3002 with Rhodamine 6G or Rhodamine Special as the dye). The fluorescence was imaged using two lenses and monitored using a photomultiplier tube fitted with a 589.5 nm interference filter (Ealing Corp. $\lambda_{\text{max}} = 589.6$, fwhm = 5 nm) or a 560 nm high pass filter. The temporal evolution of the ¹CH₂ radicals was recorded by varying the time delay between photolysis and probe lasers, a typical example of which can be seen in Fig. 1. At very short times following photolysis, probe laser excitation scans revealed the presence of rotationally excited ¹CH₂^{*}, which rapidly relaxes via reaction R13 to the temperature of the jet obtained independently by impact pressure measurements.

The reaction scheme for the formation and removal of ¹CH₂ is given by:



where ¹CH₂^{*} is an initially rotationally excited singlet methylene radical, formed in $v'' = 0$ from photolysis of the precursor, R is the co-reagent, k_{rel} is the rate coefficient for rotational relaxation of the rotationally excited single methylene radical, and k_{r} is the

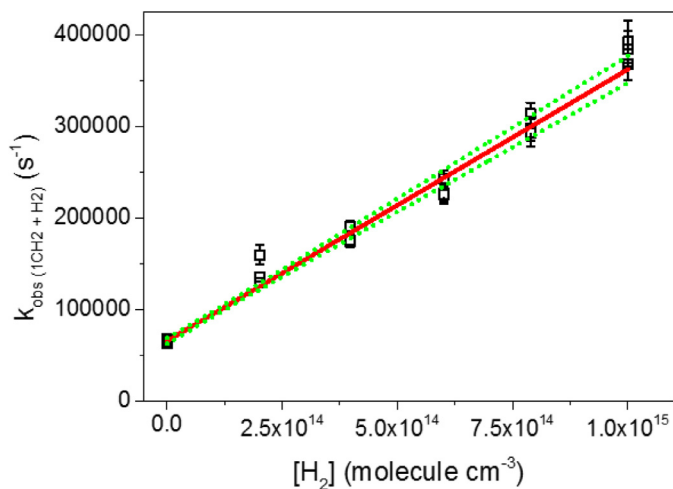


Fig. 2. Typical bimolecular plot for the removal of $^1\text{CH}_2$ with co-reactant, H_2 , at $T = (43 \pm 7)$ K, density $= (1.0 \pm 0.2) \times 10^{17}$ molecule cm^{-3} , gradient gives $k_{(1\text{CH}_2 + \text{H}_2)} = (2.96 \pm 0.15) \times 10^{-10}$ cm^3 molecule $^{-1}$ s $^{-1}$. The errors are statistical to the 2 σ level.

bimolecular rate coefficient for the reaction of singlet methylene with the co-reactant. As the experiment was carried out under pseudo-first-order conditions ($[\text{R}] \gg [^1\text{CH}_2]$), the temporal evolution of $^1\text{CH}_2$ is given by:

$$[^1\text{CH}_2]_t = \left(\frac{k_{\text{rel}}}{k_{\text{obs}} - k_{\text{rel}}} \right) [^1\text{CH}_2^*]_0 (e^{-k_{\text{rel}}t} - e^{-k_{\text{obs}}t}) + [^1\text{CH}_2]_0 e^{-k_{\text{obs}}t} \quad (\text{E1})$$

and

$$k_{\text{obs}} = k_r[\text{R}] + k_{\text{loss}} \quad (\text{E2})$$

where k_{obs} is the pseudo-first-order rate constant, t is the time (the delay between photolysis and probe laser pulses), and k_{loss} is the total rate coefficient for the other minor first order loss processes (diffusion, reaction with the ketene precursor, and relaxation via the buffer gas). Eq. (E1) was fitted to the $^1\text{CH}_2$ profiles to extract k_{obs} . A plot of k_{obs} vs $[\text{R}]$ gives a straight line of gradient k_r and intercept of k_{loss} . Fig. 2 shows an example of such a plot, and the small intercept demonstrates that the reaction with the co-reactant dominates $^1\text{CH}_2$ removal.

2.2. Branching ratio measurements

Experiments to determine the branching ratio between relaxation and reaction were carried out using the same pulsed Laval nozzle and low temperature reaction cell apparatus described above. To determine the branching ratio between relaxation and reaction, pairs of experiments were carried out in which any $^3\text{CH}_2$ produced following relaxation of $^1\text{CH}_2$ was titrated to OH with O_2 , and the amount of OH produced monitored with and without the reactive co-reactant (H_2 and CH_4) present. This scheme is summarised in Fig. 3. For experiments without the reactive co-reactant present, all $^1\text{CH}_2$ produced following pulsed photolysis of ketene was electronically relaxed to $^3\text{CH}_2$ via reactions R10 and R15.



For the reaction between $^1\text{CH}_2$ and O_2 , relaxation has been shown to be the only loss process on timescales applicable to this work (Blitz et al., 2003; Hancock and Haverd, 2003). Following relaxation of $^1\text{CH}_2$ to $^3\text{CH}_2$, the slow growth of OH from reaction R16 was then monitored.



A second experiment was then carried out, in which the reactive co-reactant is present. In this case, some of the $^1\text{CH}_2$ produced following flash photolysis of ketene may be removed by reaction (R4a and R9a) rather than relaxation, resulting in less $^3\text{CH}_2$ production and a smaller amount of OH produced following titration with O_2 .

The experimental conditions employed in determining branching ratios were such that the initial relaxation or removal of $^1\text{CH}_2$ occurred on a short timescale (< 2.5 μs) in comparison with the slow growth and subsequent loss of OH (> 100 μs). Pseudo-first-order conditions were also met, such that $[\text{O}_2] \gg [^3\text{CH}_2]$. Thus the temporal evolution of OH can be approximated by:

$$[\text{OH}]_t = \left(\frac{k_{\text{growth}}}{k_{\text{removal}} - k_{\text{growth}}} \right) [^3\text{CH}_2]_0 (e^{-k_{\text{growth}}t} - e^{-k_{\text{removal}}t}) \quad (\text{E3})$$

where k_{growth} is the pseudo-first-order rate coefficient for the reaction between $^3\text{CH}_2$ and O_2 , $[^3\text{CH}_2]_0$ is the amount of $^3\text{CH}_2$ produced by relaxation, and k_{removal} is the total rate coefficient for first order loss processes of OH (diffusion and reaction with the ketene precursor and reactive co-reactant). Thus, by monitoring the OH growth and loss, the amount of $^3\text{CH}_2$ initially produced via relaxation of $^1\text{CH}_2$ can be determined, and by comparing this value with and without the reactive co-reactant present, the amount of $^1\text{CH}_2$ being removed by reaction when the reactive co-reactant is present can be determined.

The growth and decay of OH was measured by probing the $\text{A}^2\Sigma^+(v'=0) \leftarrow \text{X}^2\Pi_i(v''=0)$, $\text{Q}_1(2)$ transition at ~ 308 nm using the frequency doubled output of an excimer pumped dye laser (Lambda Physik LPX100 pumping a Lambda Physik FL3002 with Rhodamine B). The resonant fluorescence was imaged using two lenses and monitored using a photomultiplier tube (Thorn EMI) fitted with an interference filter centred at 308.5 nm (Barr Associates, $\text{fwhm} = 5$ nm). The temporal evolution of the OH radicals was recorded by varying the time delay between photolysis and probe lasers, a typical example of which can be seen in Fig. 3. To account for any drifts in laser power between pairs of experiments, the OH signal was normalised to the probe laser power as monitored by a photodiode.

For each pair of experiments conducted, the recorded OH fluorescence signals were corrected for the differential quenching of the $\text{OH}(\text{A}^2\Sigma^+, v'=0)$ fluorescence in the presence of the reactive co-reactant compared to that recorded in the absence of the co-reactant. This was done by determining the $\text{OH}(\text{A}^2\Sigma^+, v'=0)$ fluorescence rate coefficient, k_f , for every experiment under both sets of conditions (with and without R). Using an oscilloscope, 200 fluorescence decays were averaged, and fitted to exponential profiles, $I_t = I_{t0} \exp(-k_f t)$. The ratio of the fluorescence lifetimes with and without the reactive co-reactant present would yield a correction factor, S , to be applied to the integrated OH fluorescence signals obtained with the reactive co-reactant present.

$$S = k_{f(\text{WITHR})} / k_{f(\text{WITHOUTR})} \quad (\text{E4})$$

Averaged fluorescence decays were captured for every OH growth and decay trace taken, so that individual correction factors for each pair of experiments could be determined.

In order to determine the branching ratio, the relative amounts of $^1\text{CH}_2$ reacting with the N_2/He bath gas, O_2 , and the reactive co-reactant need to be quantified. These values were taken to be the initial rates of $^1\text{CH}_2$ removal with each specie. For the experiments carried out at 160 K using the reaction cell apparatus, conditions were such that around 7% of $^1\text{CH}_2$ was removed by O_2 and the bath gases when the reactive co-reactant H_2 was present, while around 10% of $^1\text{CH}_2$ was removed by O_2 and the bath gases when the reactive co-reactant CH_4 was present. This would result in a background growth of OH that was not the result of the reactive co-reactant electronically relaxing $^1\text{CH}_2$, and has been cor-

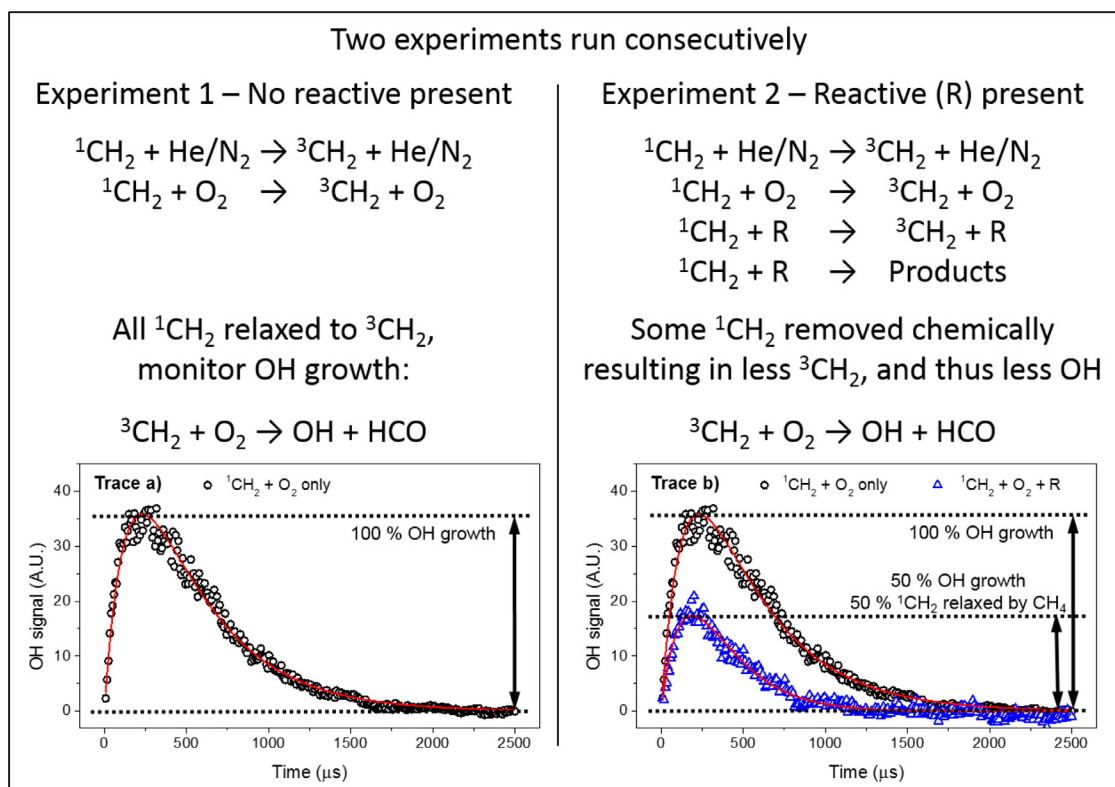


Fig. 3. Experimental scheme used to determine branching ratios by measuring OH growth from the reaction of ${}^3\text{CH}_2$ with O_2 . Traces show temporal evolution of the OH LIF signal (open symbols) together with the nonlinear least-squares fit of Eq. E3 to the data (red line) following 308 nm photolysis of ketene in the presence of a) $[\text{O}_2] = 3.3 \times 10^{15}$ and $[\text{N}_2] = 9.9 \times 10^{16}$ molecule cm^{-3} , and b) $[\text{O}_2] = 3.3 \times 10^{15}$ and $[\text{CH}_4] = 2.9 \times 10^{16}$ molecule cm^{-3} , at $T = (160 \pm 5 \text{ K})$. Plot b) has been corrected for quenching of the OH signal. Fits to Eq. E3 give a) $[{}^3\text{CH}_2]_0 = (59.7 \pm 0.9)$ A.U. and b) $[{}^3\text{CH}_2]_0 = (33.6 \pm 3.1)$ A.U., giving a ratio of ${}^3\text{CH}_2$ with and without CH_4 present of 0.56 ± 0.06 . Correcting for the amount of ${}^3\text{CH}_2$ produced by reaction of ${}^1\text{CH}_2$ with O_2 in Experiment 2 (10%) gives a branching ratio for electronic relaxation of ${}^1\text{CH}_2$ by CH_4 of 0.51 ± 0.06 . (For interpretation of the references to colour in this figure legend, the reader is referred to the web version of this article.)

rected for in our data analysis. A small amount of ${}^1\text{CH}_2$ would also have been removed by ketene *via* reaction R17; using a value of $k_{17} = 2.5 \times 10^{-10}$ cm^3 molecule $^{-1}$ s $^{-1}$ (Hancock and Heal, 1992; Hayes et al., 1996) we determine that ketene would account for less than 2.5% of ${}^1\text{CH}_2$ removal.



For the experiments carried out at 73 K using the pulsed Laval nozzle, constraints on the maximum concentration of reactants that could be introduced with the He bath gas meant that significantly more ${}^1\text{CH}_2$ was removed by O_2 and He than in the reaction cell experiments. These constraints are inherent to the Laval nozzle apparatus and could not be eliminated. Under the conditions employed in the Laval nozzle experiments, around 50% of ${}^1\text{CH}_2$ was removed by O_2 and He when the reactive co-reactant H_2 or CH_4 was present. As discussed above, this would result in a background growth of OH, which must be accounted for in the data analysis. The amount of ${}^1\text{CH}_2$ removed by ketene in the Laval nozzle experiments was less than 5%, and has been taken into consideration in the branching ratio errors reported.

3. Results

3.1. Kinetics

An example of the temporal evolution of the ${}^1\text{CH}_2$ LIF signal following 308 nm photolysis of ketene in the presence of a co-reactant, H_2 , is shown in Fig. 1. Fig. 2 gives an example of a bimolecular plot, formed by plotting k_{obs} with varying co-reactant

concentration $[\text{H}_2]$, the gradient of which yields the bimolecular rate coefficient. The bimolecular rate coefficients for the reaction of ${}^1\text{CH}_2$ with He, N_2 , O_2 , H_2 , and CH_4 , are presented in Table 2 and compared with other literature data in Fig. 4. The errors reported in this work are statistical at the 2σ level. For each temperature and co-reactant, bimolecular rate coefficients were measured at three or more different pressures (densities). No effects were observed on the bimolecular rate coefficients as pressure, radical concentration, and probe wavelength were varied.

There have been several previous studies investigating the removal rates of ${}^1\text{CH}_2$ with various colliders. All those discussed in this section below employed a similar experimental technique (PLP-LIF) and detection scheme to that used in this study. For helium (R11) there have been two temperature dependant studies by Gannon et al. (2010a) and Wagener (1990), both showing a strong positive temperature dependence, however no studies have investigated removal rates below 195 K. The rate coefficient determined at 160 K in this work is consistent with the higher temperature literature values, however below temperature a much weaker temperature dependence is seen than extrapolation of the high temperature data would suggest. Unlike the removal rates with the other co-reactants investigated in this study, no inverse temperature dependence was observed.

For nitrogen (R10), three other studies have investigated the temperature dependence down to 195 K (Gannon et al., 2010a; Hayes et al., 1996; Wagener, 1990), with all three showing a positive temperature dependence. The rate coefficients obtained at 160 and 134 K in this study are consistent with these values, however a strong inverse temperature dependence is observed at lower temperatures ($< 130 \text{ K}$) with the rate coefficient at 43 K found

Table 2

Bimolecular rate constants for the removal of $^1\text{CH}_2$ with He, N_2 , O_2 , H_2 , and CH_4 . Errors reported for the measurements made in this study are statistical at the 2σ level. Literature values taken from a) (Gannon et al., 2010a), b) (Langford et al., 1983), c) (Gannon et al., 2008), d) (Wagener, 1990).

T (K)	Rate coefficient k_r ($\text{cm}^3 \text{ molecule}^{-1} \text{ s}^{-1}$)				
	He / 10^{-12}	N_2 / 10^{-11}	O_2 / 10^{-10}	H_2 / 10^{-10}	CH_4 / 10^{-10}
43 ± 7	0.47 ± 0.09	2.59 ± 0.46	1.92 ± 0.34	2.99 ± 0.44	3.09 ± 0.48
73 ± 10	0.60 ± 0.23	2.11 ± 0.47	1.69 ± 0.28	2.14 ± 0.26	2.17 ± 0.30
84 ± 15	0.90 ± 0.27			2.16 ± 0.39	
124 ± 11		1.18 ± 0.22	1.13 ± 0.21	1.89 ± 0.33	1.84 ± 0.36
134 ± 21		0.76 ± 0.21			
160 ± 5	0.88 ± 0.38	0.84 ± 0.08	1.09 ± 0.08	1.70 ± 0.13	1.40 ± 0.15
195	1.05 ± 0.03 ^a	0.88 ± 0.05 ^a		1.03 ± 0.02 ^c	0.96 ± 0.13 ^d (T = 210 K)
298	3.33 ± 0.18 ^a	1.09 ± 0.03 ^a	0.74 ± 0.05 ^b (T = 295 K)	1.09 ± 0.06 ^c	0.76 ± 0.08 ^d (T = 295 K)

to be a factor of 3 higher than the value reported at 195 K by Gannon et al. (2010a).

There have been no temperature dependent studies of rate coefficients for $^1\text{CH}_2$ with oxygen (R15), with only two room temperature values available (Ashfold et al., 1981; Langford et al., 1983). Taking these values into account with the current work indicates the rate coefficient has a strong negative temperature dependence.

For hydrogen (R9), previous studies show little (Wagener, 1990) or no (Gannon et al., 2008; Hancock and Heal, 1992) temperature dependence above 195 K, with no previous studies reporting values below this temperature. Results from this study indicate that below 195 K, a strong negative temperature dependence is observed, with the rate coefficient at 43 K a factor or 3 higher than that reported at 195 K by Gannon et al. (2008). A similar picture is observed for methane (R4), with previous studies (Hayes et al., 1996; Wagener, 1990) showing only a modest inverse temperature dependence above 195 K, while results for this study show a much stronger inverse temperature dependence below this temperature.

In combination with the literature presented in Fig. 4, the following parameterizations have been made for the rate coefficients for the removal of $^1\text{CH}_2$:

$$\begin{aligned}
 k_{\text{He}}(43 < T/\text{K} < 800) &= (1.90 \pm 0.23) \times 10^{-12} \times (T/298)^{1.74 \pm 0.16} \\
 &\quad \times \exp^{((88 \pm 23)/T)} \\
 k_{\text{N}_2}(43 < T/\text{K} < 800) &= (2.29 \pm 1.12) \times 10^{-12} \times (T/298)^{-2.15 \pm 1.38} \\
 &\quad \times \exp^{((-74 \pm 96)/T)} + (3.91 \pm 0.78) \times 10^{-11} \times \exp^{((-469 \pm 114)/T)} \\
 k_{\text{O}_2}(43 < T/\text{K} < 300) &= (6.16 \pm 1.09) \times 10^{-11} \times (T/298)^{-0.65 \pm 0.14} \\
 k_{\text{H}_2}(43 < T/\text{K} < 800) &= (1.10 \pm 0.04) \times 10^{-10} \times (T/298)^{-0.40 \pm 0.06} \\
 &\quad \times \exp^{((11.1 \pm 6.9)/T)} \\
 k_{\text{CH}_4}(43 < T/\text{K} < 475) &= (8.20 \pm 0.46) \times 10^{-11} \times (T/298)^{-0.93 \pm 0.10} \\
 &\quad \times \exp^{((-20.5 \pm 12.8)/T)}
 \end{aligned}$$

3.2. Branching ratios

Fig. 3 shows typical temporal profiles for the study of the branching ratio between relaxation and reaction of $^1\text{CH}_2$ with a co-reactant, CH_4 . The branching ratios for electronic relaxation of $^1\text{CH}_2$ to $^3\text{CH}_2$ by H_2 and CH_4 obtained in this study are presented in Fig. 5 and Table 3 as a function of temperature, together with available literature values. There is potential for the results for the branching ratio studies to be influenced by differing $\text{OH}(v)$ quenching processes in the presence or absence of the test species (H_2 or CH_4). For hydrogen, relaxation of vibrationally excited OH is very inefficient, however, for methane vibrational relaxation of $\text{OH}(v)$ produced from the titration reaction R16, could occur on the timescales of the experiments. The potential influence of vibrational relaxation was investigated via numerical simulations and experiments as detailed in Section S1 of the Supplementary Information. The results show that there may be a small contribution to the $\text{OH}(v=0)$ signal and hence a slight over-estimation of the relaxation process. The change in the calculated branching ratios

Table 3

Branching ratio for electronic relaxation of $^1\text{CH}_2$ with H_2 and CH_4 as a function of temperature. Errors reported for the measurements made in this study represent statistical uncertainty (2σ) in the experimental data. Literature values taken from a) (Gannon et al., 2008), b) (Blitz et al., 2001), and c) (Böhland et al., 1985).

T / K	H_2	CH_4
73	0.78 ± 0.15	0.64 ± 0.19
160	0.39 ± 0.10	0.49 ± 0.09
195	0.29 ± 0.07 ^a	
298	0.15 ± 0.08 ^a 0.10 ± 0.10 ^b 0.08 ± 0.08 ^a	0.17 ± 0.08 ^c
398		
498	−0.01 ± 0.10 ^a	

between reaction and relaxation is less (e.g. 3% for the reaction of $^1\text{CH}_2$ with methane at 73 K) than the experimental uncertainty, however, the values reported for electronic relaxation should be treated as an upper limit. No effects were observed on the branching ratios as pressure, radical concentration, and reagent concentrations were varied by around a factor of two.

For hydrogen, the values measured in this work continue the observed trend that the fraction of electronic relaxation increases with decreasing temperature, with relaxation shown to account for almost 80% of $^1\text{CH}_2$ removal at 73 K, a significant increase from the 29% relaxation reported at 195 K in the literature (Gannon et al., 2008). These temperature dependent values by Gannon et al. (2008) were obtained by monitoring H atom production following reaction of $^1\text{CH}_2$ with H_2 , while the additional value at 295 K by Blitz et al. (2001) was determined by indirectly monitoring $^3\text{CH}_2$ production using a process very similar to that used in this study. As can be seen there is good agreement between the branching ratio determined by indirectly monitoring $^3\text{CH}_2$ growth and by directly monitoring H atom production.

For methane, only one room temperature branching ratio value is available in the literature. At this temperature, the branching ratio for electronic relaxation of $^1\text{CH}_2$ by CH_4 is given as 0.17 ± 0.08 (Böhland et al., 1985). This study extends the temperature range of branching ratios down to 73 K, and shows that the fraction of $^1\text{CH}_2$ removed by electronic relaxation increases with decreasing temperature, with electronic relaxation being the dominant removal channel $^1\text{CH}_2$ by CH_4 at 73 K.

4. Discussion

4.1. Titan model

To understand the implications of the measured rate coefficients and branching ratios, the results have been included in a 1D transport model of Titan's atmosphere provided by Cal-

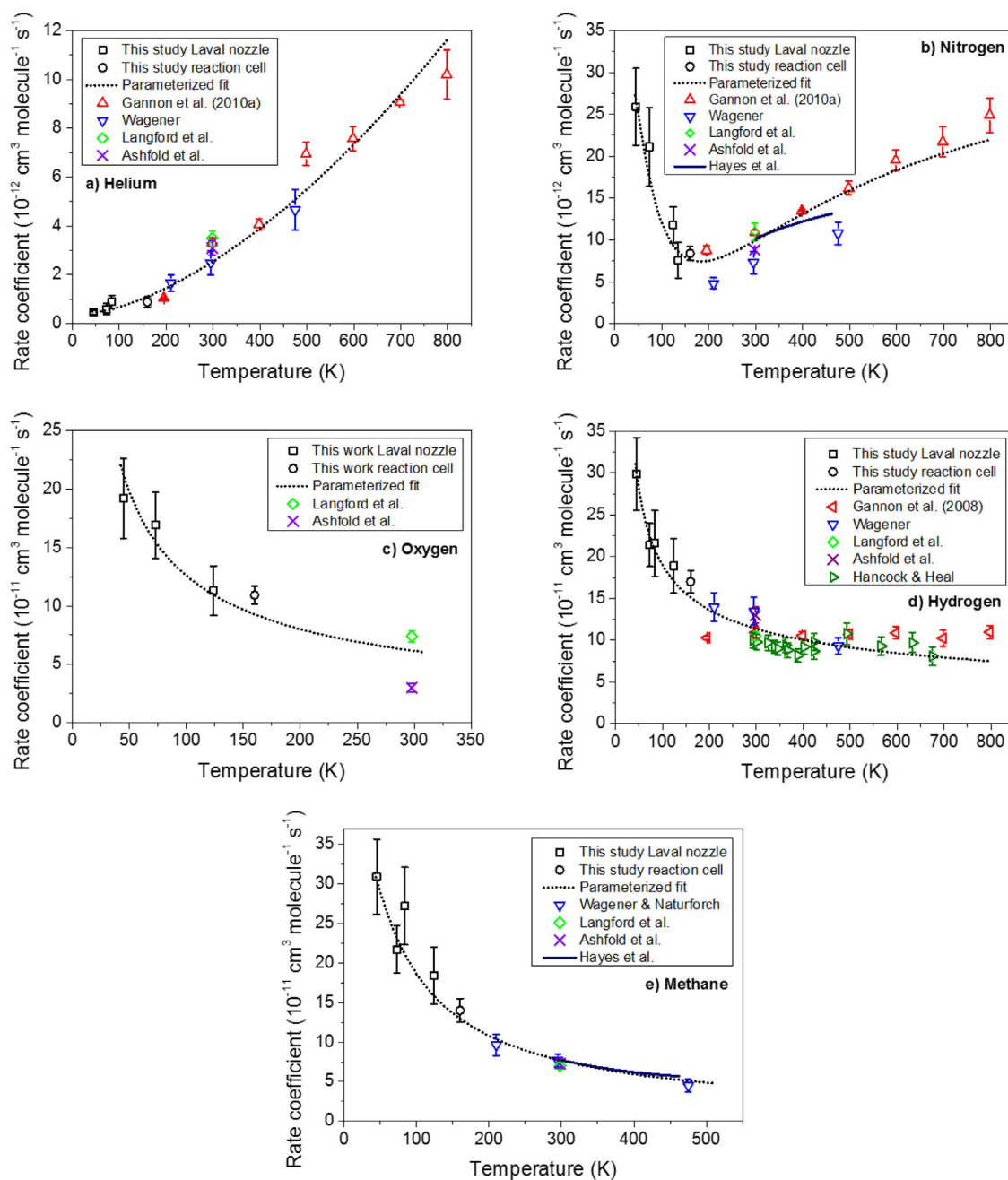


Fig. 4. Temperature dependence of the rate coefficients for $^1\text{CH}_2$ + a) helium, b) nitrogen, c) oxygen, d) hydrogen, and e) methane reported in this work and in the literature. Uncertainty ranges are given at 95% confidence. Black open squares: this study Laval nozzle experiments. Black circles: this study reaction cell experiments. Red upward triangles: (Gannon et al., 2010a). Blue downward triangles: (Wagener, 1990). Green diamonds: (Langford et al., 1983). Purple crosses: (Ashfold et al., 1981). Dark blue line: (Hayes et al., 1996). Red downward triangles: (Gannon et al., 2008). The black dotted line is a parameterization of the data. In general all the data in the figure have been used with the exception of the Wagener data for the reaction of $^1\text{CH}_2$ with N_2 . The equations can be found in the main text. (For interpretation of the references to colour in this figure legend, the reader is referred to the web version of this article.)

tech/JPL (Allen et al., 1981; Li et al., 2014; Yung, 1987; Yung et al., 1984; Zhang et al., 2010). The model contains the new set of chemical reactions from Moses et al. (2005), which was reviewed and updated with the most recent literature values, primarily from Loison et al. (2015) and Dobrijevic et al. (2016) as detailed in the Supplementary Information (Section 2). Fig. 6 shows the background atmospheric density profile, which was constructed from Cassini observations, and the eddy diffusion coefficient (K_{ZZ}) taken from Li et al. (2014), used in the model. Ion-molecule reactions are relevant to Titan's atmosphere (e.g. Vuitton et al., 2008), however, to reduce model complexity and to focus on the

results of this study, only neutral hydrocarbons and nitriles are included.

Two model runs were conducted in this work and details on the calculations and a discussion of the comparison of absolute model and measured values can be found in the Supplementary Information. The first was a base case scenario in which the most up to date literature rate coefficients for the reactions of $^1\text{CH}_2$ with N_2 (R10), H_2 (R9a and b), and CH_4 (R4a and b) were used. The second model run incorporated the low temperature rate coefficients measured in the present study. The parameterized rate coefficients

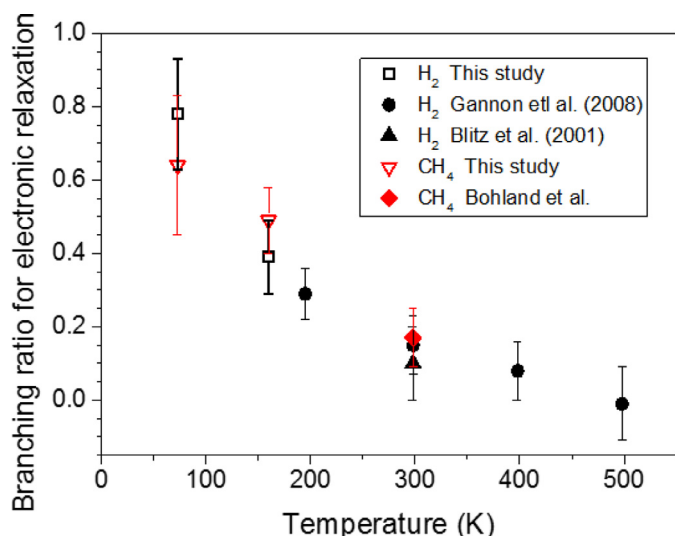


Fig. 5. Temperature dependence of the branching ratio for electronic relaxation of $^1\text{CH}_2$ with H_2 and CH_4 reported in this work and in the literature. Uncertainty ranges are given at 95% confidence. Black symbols relate to the branching ratios of H_2 ; black squares: this study. Black circles: (Gannon et al., 2008). Black upward triangles: (Blitz et al., 2001). Red symbols relate to the branching ratios of CH_4 ; black downward triangles: this study. Red diamonds: (Bohland et al., 1985). (For interpretation of the references to colour in this figure legend, the reader is referred to the web version of this article.)

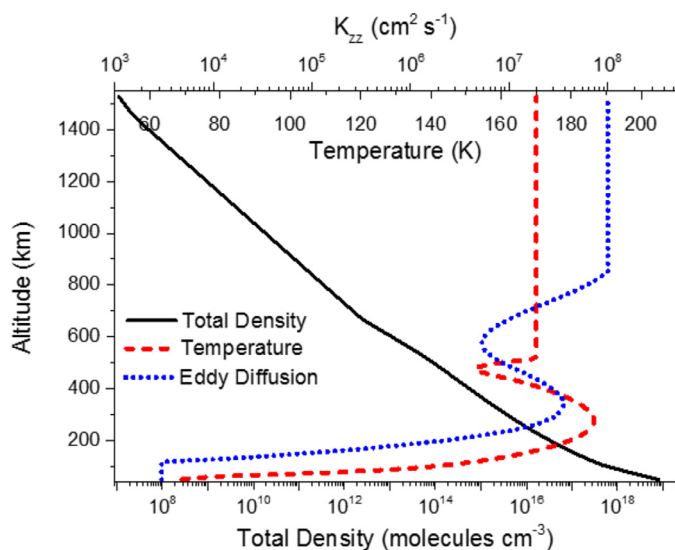


Fig. 6. Vertical profiles of total density, temperature, and eddy diffusion coefficient (K_{zz}) in the Cal-tech/JPL 1D model of Titan's atmosphere.

used in both model runs for reactions from this study can be found in Table 4.

Modelled vertical profiles obtained from both runs for some of the stable closed shell species are shown in Fig. 7, together with the observed mixing ratios. Whilst a simplified model omitting ion-molecule reactions has been used, we are more interested in the relative changes in concentrations, highlighted in this approach, rather than absolute values.

The most striking difference observed when moving from the base case scenario to this study is seen in the profile of ethane, where concentrations have decreased by 44% between 1550 and 800 km, dropping to around a 5% decrease below 400 km. This large decrease in C_2H_6 concentrations when moving from the base case scenario can be explained by the reduced amounts of CH_3 produced by reactions R4a and R9a. Fig. 8 shows the modelled rate

of CH_3 production from reactions R4a and R9a, together with rate of CH_3 recombination to form C_2H_6 . As can be seen, CH_3 production is significantly down compared to the base case scenario. As over 95% of C_2H_6 is produced by CH_3 recombination, any fall in CH_3 production results in decreased C_2H_6 production.

In contrast to the decrease in C_2H_6 concentrations, the profiles for the unsaturated hydrocarbons C_2H_2 and C_2H_4 both show small but significant increases compared with the base case scenario. Both C_2H_2 and C_2H_4 show an increase in concentration of around 5% above 600 km, rising to around 15% for C_2H_2 and 30% for C_2H_4 at 50 km, moving both profiles into better agreement with the CIRS limb and nadir observations. Despite this, observed concentrations of C_2H_2 below 250 km are still twice the modelled concentrations, while C_2H_4 observations are almost an order of magnitude higher, suggesting an underestimation of their production rates in our model although dynamical effects in Titan's atmosphere could also play a role (Hourdin et al., 2004; Teanby et al., 2012). The increase in C_2H_4 concentrations observed when moving from the base case scenario can be attributed to increased production of $^3\text{CH}_2$, the result of the increased efficiency of electronic relaxation of $^1\text{CH}_2$ by N_2 (R10), H_2 (R9b), and CH_4 (R4b) (Fig. 8). As discussed in the introduction, $^3\text{CH}_2$ is relatively unreactive with closed shell species, and is primarily lost by reactions with other radicals. Reactions with H atoms to produce CH radicals (R5) accounts for approximately 83% of $^3\text{CH}_2$ loss, while reactions with CH_3 to produce C_2H_4 (R6) accounts for approximately 8% of $^3\text{CH}_2$ loss. It could be thought that the increased amounts of $^3\text{CH}_2$ result in increased C_2H_4 production via reaction R6, however this is not the case, as the corresponding reduction in the production of methyl radicals described above, actually results in this reaction becoming less efficient when compared to the base case scenario. Instead, the reaction of $^3\text{CH}_2$ with H atoms (R5) producing methylidene, CH, radicals is in fact the cause of increased C_2H_4 , as the major loss of CH radicals is by reaction with methane (approximately 90%) to produce C_2H_4 (R7). This increase in ethylene formation is also the cause of the increased amounts of acetylene, as photolysis of C_2H_4 (R8) accounts for almost 30% of acetylene formation.

The modelled vertical profile of benzene also shows small but significant differences moving from the base case scenario. Below 500 km, an increase in C_6H_6 concentrations of up to 30% is observed, while above 500 km concentrations are lower than in the base case by approximately 5%. Modelled concentrations lie well within the CIRS nadir observations below 250 km, but are significantly lower than the concentrations determined by the INMS between 981 and 1077 km by around two orders of magnitude. A possible explanation for this discrepancy could be the exclusion of ion molecule reactions in our model. Due to the complex and interconnected nature of the reactions in our photochemical model it is difficult to fully elucidate the cause of the changes in C_6H_6 concentrations observed when moving from the base case scenario. However, the increase in benzene below 500 km in our model is shown to be the result of a series of three body reactions in which successive H atoms are added to C_6H_2 to eventually form benzene, while the increased amounts of C_6H_2 can be traced back to the increase in acetylene. It is worth noting that in a recent study from our laboratory it was shown that the cyclo-trimerization of acetylene on cosmic dust analogue particles is a potentially significant benzene source between 80 and 140 km in Titan's troposphere (Frankland et al., 2016).

4.2. Implications

The chemistry of $^1\text{CH}_2$ has been discussed in the introduction. There are two important issues to consider concerning reactions with N_2 , CH_4 and H_2 and which influence the formation of stable

Table 4
Comparison of rate coefficient expressions for the major $^1\text{CH}_2$ removal reactions (R4, 9, and 10) as used in five chemical models of Titan's atmosphere. $^3\text{CH}_2/\text{CH}_3$ is the ratio of the rate of production of the two species from the reactions listed, and $[^1\text{CH}_2]_{\text{ss}}$ is the steady state concentration of $^1\text{CH}_2$. See text for details. ^a units $\text{cm}^3 \text{ molecule}^{-1} \text{ s}^{-1}$, ^b units s^{-1} . The enhanced rate coefficients of reactions R4, R9 and R10 (both reactive loss and relaxation for the latter two reactions) determined in this study result in a lower steady-state concentration of $^1\text{CH}_2$ compared to the reactions used in all but one of the other models in Table 4. Only the reactions used in the model of Hebrard et al. (2006) predict a lower steady state concentration, primarily determined by the use of a high ($1.0 \times 10^{-11} \text{ cm}^3 \text{ molecule}^{-1} \text{ s}^{-1}$ (Baulch et al., 1992)) and temperature independent rate coefficient for reaction R10. The lower steady-state concentrations suggest that the role of other minor $^1\text{CH}_2$ reactions will be further reduced e.g. the formation of propargyl by reaction with acetylene. Additionally, if the prevalence of the relaxation over reaction channels continues for other species, then these reactions will be of less importance in building more complex molecules.

Model	$^1\text{CH}_2 + \text{N}_2$ $k(T)^a$	$k(170 \text{ K})^a$ (k'/s^{-1})		$^1\text{CH}_2 + \text{CH}_4$ $k(T)^a$	$k(170 \text{ K})^a$ (k'/s^{-1})	$^1\text{CH}_2 + \text{H}_2$ $k(T)^a$	$k(170 \text{ K})^a$ (k'/s^{-1})	$^3\text{CH}_2/\text{CH}_3$ (170 K)	$[^1\text{CH}_2]_{\text{ss}}$ /molecule cm^{-3}
Dobrijevic et al. (2016) and Loison et al. (2015)	1.1×10^{-11} , ($T/300$) ^{0.81}	6.94×10^{-12} (0.069)	Reaction	2.79×10^{-11} , $e^{(250/T)}$	1.21×10^{-10} (0.019)	8.8×10^{-11} , ($T/300$) ^{0.35}	7.21×10^{-11} (0.003)	1.74	84
			Relaxation	3.1×10^{-12} , $e^{(250/T)}$	1.35×10^{-11} (0.002)	1.6×10^{-11} , ($T/300$) ^{-0.9}	2.67×10^{-11} (0.001)		
Krasnopolsky (2009)	2.4×10^{-14} , T	4.08×10^{-12} (0.041)	Reaction	6×10^{-11}	6.00×10^{-11} (0.010)	9×10^{-11}	9.00×10^{-11} (0.004)	1.79	148
Hebrard et al. (2006)	1.0×10^{-11}	1.00×10^{-11} (0.100)	Reaction	5.9×10^{-11}	5.90×10^{-11} (0.009)	1.2×10^{-10}	1.20×10^{-10} (0.005)	4.33	69
			Relaxation	1.2×10^{-11}	1.2×10^{-11} (0.002)	1.3×10^{-11}	1.30×10^{-11} (0.001)		
(Toublanc et al., 1995)	7.9×10^{-12}	7.90×10^{-12} (0.079)	Reaction	5.9×10^{-11}	5.90×10^{-11} (0.009)	1.2×10^{-10}	1.20×10^{-10} (0.005)	3.44	84
			Relaxation	1.2×10^{-11}	1.20×10^{-11} (0.002)	1.3×10^{-11}	1.30×10^{-11} (0.001)		
Base case scenario	1.1×10^{-11} , ($T/300$) ^{0.81}	6.94×10^{-12} (0.069)	Reaction	2.66×10^{-11} , $e^{(265/T)}$	1.26×10^{-10} (0.020)	8.8×10^{-11} , ($T/300$) ^{0.35}	7.21×10^{-11} (0.003)	1.72	82
			Relaxation	5.44×10^{-12} , $e^{(265/T)}$	2.59×10^{-11} (0.004)	1.6×10^{-11} , ($T/300$) ^{-0.9}	2.67×10^{-11} (0.001)		
This work	6.1×10^{-12} , ($T/300$) ^{0.13} , $e^{(78/T)}$	8.96×10^{-12} (0.090)	Reaction	6.65×10^{-11} , ($T/300$) ^{-0.056} , $e^{(0.6/T)}$	6.89×10^{-11} (0.011)	1.42×10^{-10} , ($T/300$) ^{-0.193} , $e^{(-118/T)}$	7.91×10^{-11} (0.003)	3.98	70
			Relaxation	2.48×10^{-11} , ($T/300$) ^{-2.917} , $e^{(-154/T)}$	5.26×10^{-11} (0.008)	2.53×10^{-11} , ($T/300$) ^{-2.709} , $e^{(-126/T)}$	5.62×10^{-11} (0.002)		

products; firstly the partitioning of $^1\text{CH}_2$ between $^3\text{CH}_2$ and CH_3 and secondly the steady-state concentration of $^1\text{CH}_2$. First, $^3\text{CH}_2$ is formed via collisional relaxation with N_2 (R10) and in the collisional relaxation components of the reactions with methane (R4b), hydrogen (R9b) and other hydrocarbons. CH_3 is formed from the reactive components of the reactions of $^1\text{CH}_2$ with methane (R4a) and hydrogen (R9a). Secondly, the rate of minor, but important, removal processes of $^1\text{CH}_2$, such as the reaction with C_2H_2 forming the propargyl radical (a precursor to benzene) will depend on the steady state concentration of $^1\text{CH}_2$, $[^1\text{CH}_2]_{\text{ss}}$. For fixed methane and methyl photolysis rates to form $^1\text{CH}_2$ (taken from Wilson and Atreya, 2000), $[^1\text{CH}_2]_{\text{ss}}$ will be determined primarily by the rates of removal with N_2 , CH_4 and H_2 . Therefore the relative competition between reaction and relaxation in reactions R4 and R9 is critical in determining the $^3\text{CH}_2/\text{CH}_3$ production rate ratios from $^1\text{CH}_2$, and the absolute rate of $^1\text{CH}_2$ removal determines $[^1\text{CH}_2]_{\text{ss}}$ and hence the importance of reactions such as $^1\text{CH}_2$ with C_2H_2 (R3).

Table 4 compares the rate coefficient expressions for the major $^1\text{CH}_2$ removal reactions as used in five chemical models of Titan's atmosphere. A similar table for the atmospheres of the giant planets Uranus and Neptune can be found in the supplementary information. The ratio of $^3\text{CH}_2/\text{CH}_3$ is given by the fate of photolytically produced $^1\text{CH}_2$ (photolysis rate = $8 \text{ molecule cm}^3 \text{ s}^{-1}$ at 1000 km, Wilson and Atreya (2000)) determined by comparing the rates of $^3\text{CH}_2$ and CH_3 production at 170 K and an altitude of 1000 km and with concentrations of N_2 ($1 \times 10^{10} \text{ molecule cm}^{-3}$), CH_4 ($1.6 \times 10^8 \text{ molecule cm}^{-3}$) and H_2 ($4 \times 10^7 \text{ molecule cm}^{-3}$) from Krasnopolsky (2009):

rate of $^3\text{CH}_2$ production

rate of CH_3 production

$$= \frac{k_{10}[^1\text{CH}_2][\text{N}_2] + k_{4b}[^1\text{CH}_2][\text{CH}_4] + k_{9b}[^1\text{CH}_2][\text{H}_2]}{2 \times k_{4a}[^1\text{CH}_2][\text{CH}_4] + k_{9a}[^1\text{CH}_2][\text{H}_2]}$$

$$= \frac{k_{10}[\text{N}_2] + k_{4b}[\text{CH}_4] + k_{9b}[\text{H}_2]}{2 \times k_{4a}[\text{CH}_4] + k_{9a}[\text{H}_2]}$$

The steady-state concentration of $^1\text{CH}_2$ was calculated from:

rate of $^1\text{CH}_2$ photolytic production

$$= k_{10}[^1\text{CH}_2]_{\text{ss}}[\text{N}_2] + k_4[^1\text{CH}_2]_{\text{ss}}[\text{CH}_4] + k_9[^1\text{CH}_2]_{\text{ss}}[\text{H}_2]$$

$$[^1\text{CH}_2]_{\text{ss}} = \frac{8.0}{k_{10}[\text{N}_2] + k_4[\text{CH}_4] + k_9[\text{H}_2]}$$

Values of $^3\text{CH}_2/\text{CH}_3$ production rates range from 1.72 to 4.33 for a temperature of 170 K and an altitude of 1000 km for different Titan models. There are three low values: 1.74 Dobrijevic et al. (2016), 1.79 Krasnopolsky (2009), and 1.72 from the base case scenario model used in this study. Examination of Table 4 shows that the three low ratios derive from the relative importance of the reactive component of reaction R4 leading to two methyl radicals, compared to electronic quenching via collisions with nitrogen (R10). However, in the more recent model of Dobrijevic et al. (2016), consideration of the negative temperature of reaction R4 which we believe are based on the measurements of Hayes et al. (1996), leads to a significantly higher fraction of $^1\text{CH}_2$ being removed by methane. Conversely in the Krasnopolsky model, the rate coefficient of R4 is based on the room temperature measurement of Böhland et al. (1985), approximately a factor two lower than that used in the Dobrijevic et al. (2016) model. The resultant effect on $[\text{CH}_2]_{\text{ss}}$ is compensated by the low

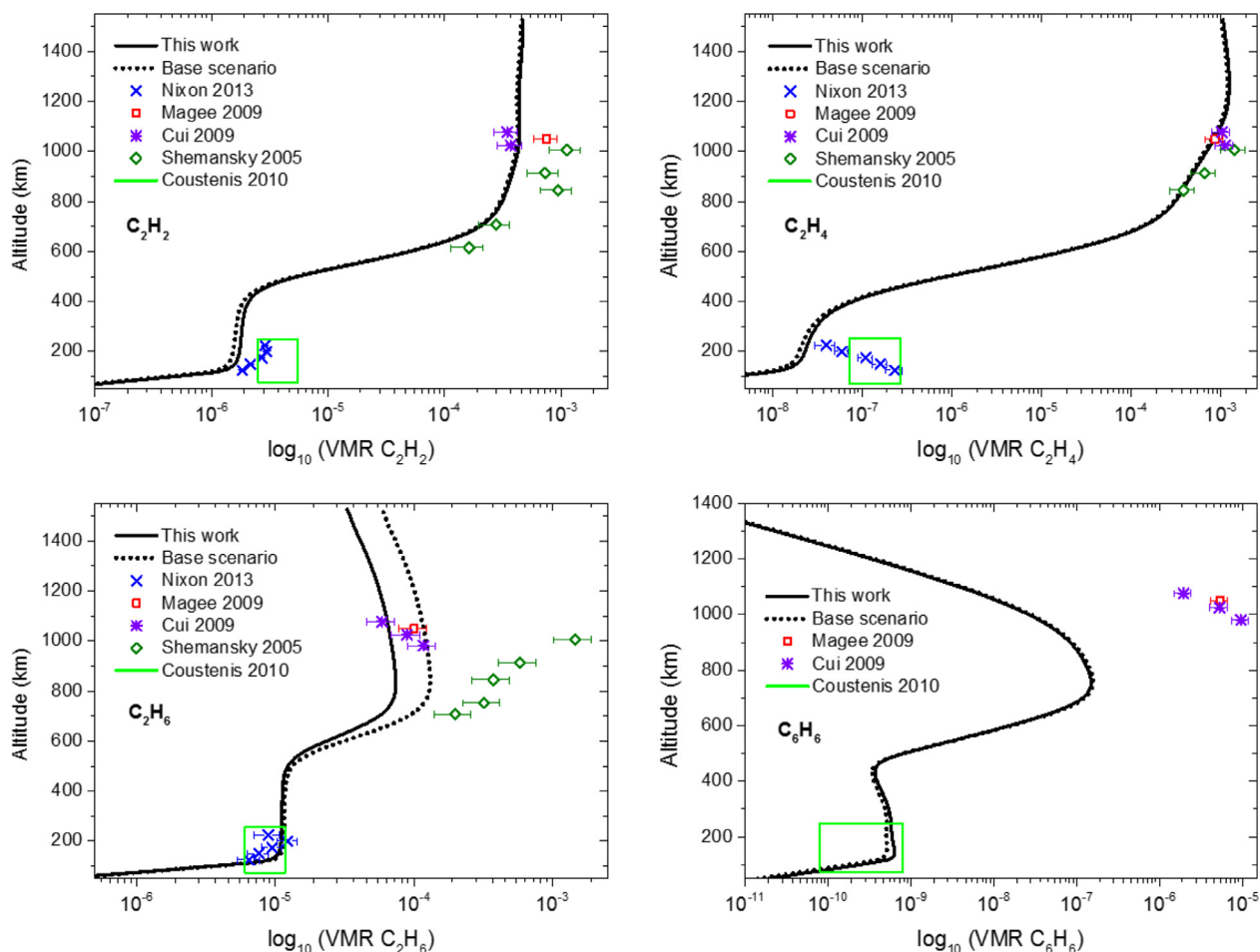


Fig. 7. Modelled vertical mixing ratio (VMR) profiles for both the base case scenario (dashed black lines) and using the rate coefficients determined in this study (solid black lines), and comparison with observations. Blue crosses: CIRS Limb (Nixon et al., 2013). Red squares: INMS (Magee et al., 2009). Purple stars: INMS (Cui et al., 2009). Dark green triangles: UVIS (Shemansky et al., 2005). Light green box: CIRS Nadir (Coustenis et al., 2010). (For interpretation of the references to colour in this figure legend, the reader is referred to the web version of this article.)

rate coefficient for reaction R10 (${}^1\text{CH}_2 + \text{N}_2$), $k_{10} = 2.4 \times 10^{-14} \times T$. This expression is based on the room temperature measurement reported by Ashfold et al. (1981), and presumably on the temperature dependence (300–859 K) for ${}^1\text{CH}_2 + \text{Ar}$, reported by Hancock and Heal (1992). The models of Hebrard et al. (2006) and Toubblanc et al. (1995) report significantly higher ratios due to higher, temperature independent rate coefficients for reaction R10, whilst using the Böhlend et al. (1985) rate coefficient for reaction R4a.

Our measurements of the removal rate of ${}^1\text{CH}_2$ with H_2 and CH_4 confirm the enhancement of the rate coefficients with decreasing temperature, but crucially also confirm our earlier measurements (Gannon et al., 2010b, 2008) of the decreasing importance of the reactive component at lower temperatures. Based on our observations of the OH signal arising from the slow reaction of ${}^3\text{CH}_2$ with O_2 , we determine that relaxation is the dominant channel for reactions R4 and R9 at 73 K, leading to significant partitioning of ${}^1\text{CH}_2$ into ${}^3\text{CH}_2$ with limited production of CH_3 .

Reaction 4a is a significant source of methyl radicals, the recombination of which is the predominance source of ethane on Titan. Thus as discussed above, any reduction in the efficiency of reaction 4a will result in a commensurate reduction in ethane production. The conversion of reactive ${}^1\text{CH}_2$ to relatively unreactive ${}^3\text{CH}_2$ is not the termination of radical chemistry. Reaction R5 converts ${}^3\text{CH}_2$ into reactive CH radicals which can undergo a range of reactions including the conversion of methane into ethane (R7)

and other insertion/elimination reactions, e.g. reaction R12 (McKee et al., 2003; Trevitt et al., 2013), which lead to complex radical species such as C_3H_2 .



The rate coefficients of reaction R10 measured in this work are all higher than would be predicted by an extrapolation of our earlier work based on measurements over the temperature range 195–700 K, with the values measured at 124 K and below being 2–5 times higher than predicted. Previous studies in this laboratory at higher temperatures had observed different rate coefficients for the relaxation of ortho and para ${}^1\text{CH}_2$, consistent with the number of gateway states between singlet and triplet in the ortho and para ro-vibrational manifolds (Gannon et al., 2010a). As well as measuring enhanced rate coefficients, no ortho, para dependence in our low temperature studies was observed, despite extensive measurements of both states. We interpret both the loss of any ortho/para effect and the enhancement of the rate coefficient as being due to the formation of complexes. Fig. 4 shows the temperature dependence of the rate coefficients for the removal of ${}^1\text{CH}_2$ with He, O_2 , N_2 , H_2 , and CH_4 , and it can be seen that the enhancement of the rate coefficients at low temperatures decreases in the same order as the binding energy of the complexes, i.e. CH_4 (12.1 K) > O_2

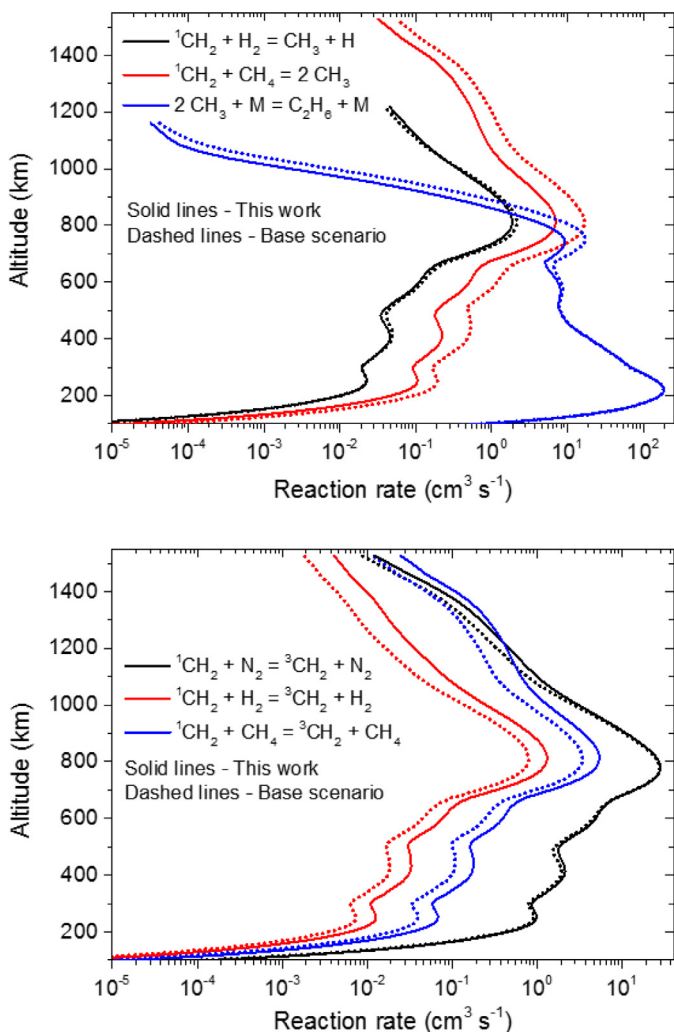


Fig. 8. A comparison of modelled reaction rates as a function of altitude, for the base case scenario (dashed lines) and using the rates determined in this study (solid lines).

(10.8 K) > N₂ (9.7 K) > H₂ (6.1 K) > He (3.2 K) where the values in brackets are the bind energies of the dimers divided by the Boltzmann constant which will be proportional to the magnitude of the CH₂ – substrate interaction (Lin et al., 1979). As the singlet and triplet states of methylene have slightly different shaped potential energy surfaces, complex formation results in different singlet and triplet states being brought into co-incidence, effectively washing out the ortho, para effects.

For the giant planets Uranus and Neptune (see Supplementary Information Section 3), both of which consist primarily of hydrogen (80–85%) with only trace amounts of methane (<0.02%) in their upper atmospheres, it is the rate of reaction R9 that will have the most significant effect on the ratio of ³CH₂:CH₃ and the steady-state concentration of ¹CH₂ in their atmospheres. For Uranus and Neptune at altitudes corresponding to 1 mbar pressure (T = 75 K Uranus, 130 K Neptune), using the rate coefficients from the photochemical model of Lee et al. (2000) gives a ³CH₂:CH₃ ratio of 0.18 for both planets (no temperature dependence for competition between reaction and relaxation for R9). Using the rate coefficients determined in this study results in an increase in the ratio of ³CH₂:CH₃ production from ¹CH₂ on both planets; for Neptune an increase of around 8 times, while the colder temperatures on Uranus results in an increase of a factor of 30. Both planets also see reductions in their [¹CH₂]_{SS} when moving to the rate coeffi-

cients determined in this study, with all values for [¹CH₂]_{SS} being significantly lower than for Titan due to the fast removal by H₂.

5. Summary

The rate coefficients for the reactions of ¹CH₂ with He, O₂, N₂, CH₄ and H₂ have been measured in a pulsed Laval system between 43 and 134 K. With the exception of He, all rate coefficients demonstrate a negative temperature dependence. The enhanced removal of ¹CH₂ by these colliders at low temperatures appears to be correlated with the well depth of the ¹CH₂ – Reagent complex and the loss of any ortho/para dependence is also consistent with complex formation influencing the reaction mechanism.

For the reactions with CH₄ and H₂ there is a competition between reaction and relaxation. Our studies demonstrate that whilst the absolute magnitude of ¹CH₂ removal is enhanced, reduced temperatures lead to electronic relaxation to ³CH₂ becoming the dominant channel.

The role of the enhanced formation of ³CH₂ over other possible products has been explored using a 1D chemistry, transport model of Titan's atmosphere and it has been shown to lead to reduced amounts of ethane (between 10 and 50%) and increased amounts of both ethene and acetylene (around 5%). The reduced amounts of ethane are the direct result of reductions in CH₃ formation via reactions of ¹CH₂ with methane (R4a) and hydrogen (R9a) while the increases in the ethene and acetylene are due to conversion of ³CH₂ first to CH with H atoms (R5), and then onto ethene by reaction methane (R7).

Acknowledgements

We thank the STFC (grant ST/L0006281/) for funding for KD. KW's work was conducted at the Jet Propulsion Laboratory, California Institute of Technology under contract with the National Aeronautics and Space Administration.

Supplementary materials

Supplementary material associated with this article can be found, in the online version, at doi:10.1016/j.icarus.2017.12.023.

References

- Allen, M., Yung, Y.L., Waters, J.W., 1981. Vertical transport and photochemistry in the terrestrial mesosphere and lower thermosphere (50–120 km). *J. Geophys. Res. (Space Phys.)*, 86, 3617–3627.
- Arendale, W.F., Fletcher, W.H., 1957. Infrared spectra of ketene and deuteroketenes. *J. Chem. Phys.* 26, 793–797.
- Ashfold, M.N.R., Fullstone, M.A., Hancock, G., Ketley, G.W., 1981. Singlet methylene kinetics - direct measurements of removal rates of (^a1A₁) and (^b1B₁) CH₂ and CD₂. *Chem. Phys.* 55, 245–257.
- Baulch, D.L., et al., 1992. Evaluated kinetic data for combustion modelling. *J. Phys. Chem. Ref. Data.* 21, 411–734.
- Bley, U., Temps, F., 1993. Collision induced intersystem crossing of CH₂: a case study of the mixed-state model. *J. Chem. Phys.* 98, 1058–1072.
- Blitz, M.A., Johnson, D.G., Pesa, M., Pilling, M.J., Robertson, S.H., Seakins, P.W., 1997. Reaction of CH radicals with methane isotopomers. *J. Chem. Soc., Faraday Trans.* 93, 1473–1479.
- Blitz, M.A., McKee, K.W., Pilling, M.J., Seakins, P.W., 2003. Evidence for the dominance of collision-induced intersystem crossing in collisions of ¹CH₂ with O₂ and a determination of the H atom yields from ³CH₂ + O₂, using time-resolved detection of H formation by vuvLIF. *Chem. Phys. Lett.* 372, 295–299.
- Blitz, M.A., Pilling, M.J., Seakins, P.W., 2001. Collision induced intersystem crossing in methylene on reactive surfaces: application of a new technique to CH₂(^a1A₁) + H₂. *Phys. Chem. Chem. Phys.* 3, 2241–2244.
- Blitz, M.A., Seakins, P.W., 2012. Laboratory studies of photochemistry and gas phase radical reaction kinetics relevant to planetary atmospheres. *Chem. Soc. Rev.* 41, 6318–6347.
- Böhland, T., Temps, F., Wagner, H.G., 1985. The contributions of intersystem crossing and reaction in the removal of CH₂(^a1A₁) by hydrocarbons studied with LMR. *Ber. Bunsen. Phys. Chem.* 89, 1013–1018.
- Brownsword, R.A., et al., 1997. Kinetics over a wide range of temperature (13–744 K): rate constants for the reactions of CH(n=0) with H₂ and D₂ and for the removal of CH(n=1) by H₂ and D₂. *J. Chem. Phys.* 106, 7662–7677.

- Canosa, A., Sims, I.R., Travers, D., Smith, I.W.M., Rowe, B.R., 1997. Reactions of the methylidene radical with CH_4 , C_2H_2 , C_2H_4 , C_2H_6 , and but-1-ene studied between 23 and 295 K with a CRESU apparatus. *Astron. Astrophys.* 323, 644–651.
- Caravan, R.L., Shannon, R.J., Lewis, T., Blitz, M.A., Heard, D.E., 2015. Measurements of rate coefficients for reactions of OH with ethanol and propan-2-ol at very low temperatures. *J. Phys. Chem. A* 119, 7130–7137.
- Coustenis, A., et al., 2010. Titan trace gaseous composition from CIRS at the end of the Cassini–Huygens prime mission. *Icarus* 207, 461–476.
- Cui, J., et al., 2009. Analysis of Titan's neutral upper atmosphere from Cassini Ion Neutral Mass Spectrometer measurements. *Icarus* 200, 581–615.
- Dobrijevic, M., Loison, J.C., Hickson, K.M., Gronoff, G., 2016. 1D-coupled photochemical model of neutrals, cations and anions in the atmosphere of Titan. *Icarus* 268, 313–339.
- Fisher, G.J., Maclean, A.F., Schnizer, A.W., 1953. Apparatus for the preparation of Ketene by the Pyrolysis of Acetic Anhydride. *J. Org. Chem.* 18, 1055–1057.
- Frankland, V.L., et al., 2016. Uptake of acetylene on cosmic dust and production of benzene in Titan's atmosphere. *Icarus* 278, 88–99.
- Gannon, K.L., Blitz, M.A., Kovács, T., Pilling, M.J., Seakins, P.W., 2010a. State resolved measurements of a $^1\text{CH}_2$ removal confirm predictions of the gateway model for electronic quenching. *J. Chem. Phys.* 132, 024302.
- Gannon, K.L., et al., 2010b. An experimental and theoretical investigation of the competition between chemical reaction and relaxation for the reactions of $^1\text{CH}_2$ with acetylene and ethene; implications for the chemistry of the giant planets. *Faraday Discuss* 147, 173–188.
- Gannon, K.L., Blitz, M.A., Liang, C.H., Pilling, M.J., Seakins, P.W., Glowacki, D.R., 2010c. Temperature dependent kinetics (195–798 K) and H atom yields (298–498 K) from reactions of $^1\text{CH}_2$ with acetylene, ethene, and propene. *J. Phys. Chem. A* 114, 9413–9424.
- Gannon, K.L., Blitz, M.A., Pilling, M.J., Seakins, P.W., Klippenstein, S.J., Harding, L.B., 2008. Kinetics and product branching ratios of the reaction of $^1\text{CH}_2$ with H_2 and D_2 . *J. Phys. Chem. A* 112, 9575–9583.
- Gans, B., et al., 2011. Photolysis of methane revisited at 121.6 nm and at 118.2 nm: quantum yields of the primary products, measured by mass spectrometry. *Phys. Chem. Chem. Phys.* 13, 8140–8152.
- Gomez Martin, J.C., Caravan, R.L., Blitz, M.A., Heard, D.E., Plane, J.M.C., 2014. Low temperature kinetics of the $\text{CH}_3\text{OH} + \text{OH}$ reaction. *J. Phys. Chem. A* 118, 2693–2701.
- Hancock, G., Haverd, V., 2003. A time-resolved FTIR emission study of the gas phase removal processes of $\text{CH}_2(X^3B_1)$ and $\text{CH}_2(a^1A_1)$ in collisions with O_2 . *Chem. Phys. Lett.* 372, 288–294.
- Hancock, G., Heal, M.R., 1992. Temperature dependences of $\text{CH}_2(a^1A_1)$ removal rates by Ar, NO, H_2 , and CH_2CO in the range 295–859 K. *J. Phys. Chem.* 96, 10316–10322.
- Hayes, F., Lawrance, W.D., Staker, W.S., King, K.D., 1996. Temperature dependences of singlet methylene removal rates. *J. Phys. Chem.* 100, 11314–11318.
- Hebrard, E., Dobrijevic, M., Benilan, Y., Raulin, F., 2006. Photochemical kinetics uncertainties in modeling Titan's atmosphere: a review. *J. Photochem. Photobiol. C-Photochem. Rev.* 7, 211–230.
- Hourdin, F., Lebonnois, S., Luz, D., Rannou, P., 2004. Titan's stratospheric composition driven by condensation and dynamics. *J. Geophys. Res. (Planets)* 109.
- Jensen, P., Bunker, P.R., 1988. The potential surface and stretching frequencies of X^3B_1 methylene (CH_2) determined from experiment using the Morse oscillator-rigid bender internal dynamics Hamiltonian. *J. Chem. Phys.* 89, 1327–1332.
- Krasnopolsky, V.A., 2009. A photochemical model of Titan's atmosphere and ionosphere. *Icarus* 201, 226–256.
- Langford, A.O., Petek, H., Moore, C.B., 1983. Collisional removal of $\text{CH}_2(^1A_1)$: absolute rate constants for atomic and molecular collisional partners at 295 K. *J. Chem. Phys.* 78, 6650–6659.
- Lee, A.Y.T., Yung, Y.L., Moses, J., 2000. Photochemical modeling of CH_3 abundances in the outer solar system. *J. Geophys. Res. (Planets)* 105, 20207–20225.
- Li, C., Zhang, X., Kammer, J.A., Liang, M.C., Shia, R.L., Yung, Y.L., 2014. A non-monotonic eddy diffusivity profile of Titan's atmosphere revealed by Cassini observations. *Planet. Space Sci.* 104, 48–58.
- Lin, H.M., Seaver, M., Tang, K.Y., Knight, A.E.W., Parmenter, C.S., 1979. *J. Chem. Phys.* 70, 5442–5457.
- Loison, J.C., et al., 2015. The neutral photochemistry of nitriles, amines and imines in the atmosphere of Titan. *Icarus* 247, 218–247.
- Lorenz, R.D., 2014. In: Müller-Wodarg, I., Griffith, C.A., Lellouch, E., Cravens, T.E. (Eds.). In: Titan: Interior, Surface, Atmosphere, and Space Environment, 49. Cambridge University Press, Cambridge, UK, pp. 1139–1140. 2014, ISBN #978-0521199926). *Meteoritics & Planetary Science*.
- Magee, B.A., Waite, J.H., Mandt, K.E., Westlake, J., Bell, J., Gell, D.A., 2009. IN-MS-derived composition of Titan's upper atmosphere: analysis methods and model comparison. *Planet. Space Sci.* 57, 1895–1916.
- McKee, K., et al., 2003. H atom branching ratios from the reactions of CH with C_2H_2 , C_2H_4 , C_2H_6 , and neo- C_5H_{12} at room temperature and 25 Torr. *J. Phys. Chem. A* 107, 5710–5716.
- Mordant, D.H., et al., 1993. Primary product channels in the photodissociation of methane at 121.6 nm. *J. Chem. Phys.* 98, 2054–2065.
- Morgan, C.G., Drabells, M., Wodtke, A.M., 1996. The correlated product state distribution of ketene photodissociation at 308 nm. *J. Chem. Phys.* 104, 7460–7474.
- Moses, J.I., Fouchet, T., Bezard, B., Gladstone, G.R., Lellouch, E., Feuchtgruber, H., 2005. Photochemistry and diffusion in Jupiter's stratosphere: constraints from ISO observations and comparisons with other giant planets. *J. Geophys. Res. (Space Phys.)* 110.
- Nixon, C.A., et al., 2013. Detection of propene in Titan's stratosphere. *Astrophys. J. Lett.* 776, L14.
- Rowe, B.R., Marquette, J.B., 1987. CRESU studies of ion molecule reactions. *Int. J. Mass Spectrom. Ion Processes.* 80, 239–254.
- Shannon, R.J., Blitz, M.A., Goddard, A., Heard, D.E., 2013. Accelerated chemistry in the reaction between the hydroxyl radical and methanol at interstellar temperatures facilitated by tunnelling. *Nat. Chem.* 5, 745–749.
- Shannon, R.J., Taylor, S., Goddard, A., Blitz, M.A., Heard, D.E., 2010. Observation of a large negative temperature dependence for rate coefficients of reactions of OH with oxygenated volatile organic compounds studied at 86–112 K. *Phys. Chem. Chem. Phys.* 12, 13511–13514.
- Shemansky, D.E., Stewart, A.I.F., West, R.A., Esposito, L.W., Hallett, J.T., Liu, X.M., 2005. The Cassini UVIS stellar probe of the Titan atmosphere. *Science* 308, 978–982.
- Sims, I.R., Smith, I.W.M., 1995. Gas-phase reactions and energy-transfer at very-low temperatures. *Ann. Rev. Phys. Chem.* 46, 109–137.
- Smith, I.W.M., 2006. Reactions at very low temperatures: gas kinetics at a new frontier. *Angew. Chem., Int. Ed.* 45, 2842–2861.
- Smith, I.W.M., Sage, A.M., Donahue, N.M., Herbst, E., Quan, D., 2006. The temperature-dependence of rapid low temperature reactions: experiment, understanding and prediction. *Faraday Discuss* 133, 137–156.
- Smith, N.S., Raulin, F., 1999. Modeling of methane photolysis in the reducing atmospheres of the outer solar system. *J. Geophys. Res. (Planets)* 104, 1873–1876.
- Taylor, S.E., Goddard, A., Blitz, M.A., Cleary, P.A., Heard, D.E., 2008. Pulsed laser nozzle study of the kinetics of OH with unsaturated hydrocarbons at very low temperatures. *Phys. Chem. Chem. Phys.* 10, 422–437.
- Teanby, N.A., et al., 2012. Active upper-atmosphere chemistry and dynamics from polar circulation reversal on Titan. *Nature* 491, 732–735.
- Thiesemann, H., MacNamara, J., Taatjes, C.A., 1997. Deuterium kinetic isotope effect and temperature dependence in the reactions of CH_2^2P with methane and acetylene. *J. Phys. Chem. A* 101, 1881–1886.
- Toublanc, D., Parisot, J.P., Brillet, J., Gautier, D., Raulin, F., McKay, C.P., 1995. Photochemical modeling of Titan's atmosphere. *Icarus* 113, 2–26.
- Trevitt, A.J., et al., 2013. Product branching fractions of the CH plus propene reaction from synchrotron photoionization mass spectrometry. *J. Phys. Chem. A* 117, 6450–6457.
- Vuitton, V., Yelle, R.V., Cui, J., 2008. Formation and distribution of benzene on Titan. *J. Geophys. Res. (Planets)* 113.
- Wade, E.A., Clauberg, H., Kim, S.K., Mellinger, A., Moore, C.B., 1997. Dynamics of rotational energy release for dissociation of singlet ketene and the singlet/triplet branching ratio. *J. Phys. Chem. A* 101, 732–739.
- Wagener, R., 1990. Influence of the temperature on the removal rates of $\text{CH}_2(a^1A_1)$ by inter-gases and hydrocarbons. *Z. Naturforsch. Sect. A. J. Phys. Sci.* 45, 649–656.
- Wilson, E.H., Atreya, S.K., 2000. Sensitivity studies of methane photolysis and its impact on hydrocarbon chemistry in the atmosphere of Titan. *J. Geophys. Res. (Planets)* 105, 20263–20273.
- Wilson, E.H., Atreya, S.K., 2003. Chemical sources of haze formation in Titan's atmosphere. *Planet. Space Sci.* 51, 1017–1033.
- Yung, Y.L., 1987. An update of nitrile photochemistry on Titan. *Icarus* 72, 468–472.
- Yung, Y.L., Allen, M., Pinto, J.P., 1984. Photochemistry of the atmosphere of Titan – comparison between model and observations. *Astrophys. J. Suppl. Ser.* 55, 465–506.
- Zhang, X., Ajello, J.M., Yung, Y.L., 2010. Atomic carbon in the upper atmosphere of Titan. *Astrophys. J. Lett.* 708, L18–L21.